Exploring the Limitations of X-ray Reflectivity as a Critical Dimension Pattern Shape Metrology*

Hae-Jeong Lee§, Sangcheol Kim, Christopher L. Soles, Eric K. Lin, and Wen-li Wu

National Institute of Standards and Technology, Polymers Division,
100 Bureau Drive, MS 8541, Gaithersburg, MD 20899

ABSTRACT

Specular X-ray reflectivity (SXR) can be used, in the limit of the effective medium approximation (EMA), as a high-resolution shape metrology for periodic and irregular patterns on a smooth substrate. The EMA defines as that the density of the solid pattern and the space separating the patterns are averaged together. In this limit the density profile as a function of pattern height obtained by SXR can be used to extract quantitative information on the cross-sectional pattern profile. Here we explore the limitations of SXR as a pattern shape metrology by studying diblock copolymer films with irregularly shaped bicontinuous terraces on quantized flat layers alternating with two polymer blocks. We conclude that SXR can be extended to irregular shaped patterns encountered in current electronic devices as long as average lateral length scale is smaller than coherence length of X-ray source. The detailed cross-sectional profiles of irregular patterns are discussed along with atomic force microscope results.

Keywords: X-ray reflectivity, effective medium approximation, pattern shape metrology, irregular shape, block copolymer, cross-sectional profile, atomic force microscope

1. INTRODUCTION

Patterned structures are utilized in range of devices, including semiconductors, optical communications elements, data storage, bio-sensors, nano-fluidics, and organic thin film transistors. Common to the manufacturing of these technologies is a need to precisely characterize and control the physical shape of the patterns. However, characterizing the pattern shape can be a challenge, especially in the limit of nanoscale structures that require not only high-resolution and accuracy, but also preferably non-destructive measurement techniques. Recently we demonstrated that specular X-ray reflectivity (SXR), when complimented by critical dimension-small angle X-ray scattering (CD-SAXS), can be a powerful methodology to quantify the complete cross section of periodic nano and micron line gratings.[1-3] To utilize SXR as a pattern metrology, the coherence length of incident X-ray beam should be greater than the characteristic dimensions of the patterned structures being investigated. In this limit the effective medium approximation (EMA) holds and the X-rays measure an average density, averaged over both the lines and spaces, for the patterned region. The basis of EMA is illustrated in Figure 1. When the coherence length of the X-ray source is larger than the physical dimensions of the patterns, the density of the lines and spaces (for a grating structure) are averaged together as one "effective" density, thus the EMA. For periodic patterns (such as the gratings shown here), this effective density contains quantitative information about the line-to-space ratio. Since the effective density is reduced proportionally by volume fraction defined by the line-to-space ratio, the line-to-space ratio can be deduced as a function of pattern height by fit SXR data with a multilayer recursive model. The opposite extreme would be the limit where the length scales of the surface patterns are larger than the coherence length of the X-rays at which point the surface begins to look physically "rough." In this respect the utility of SXR as a pattern shape metrology is limited to patterns where the periodicity is smaller than the coherence length of the X-ray source. It should be noted that modeling ellipsometry or scatterometry results to characterize pattern shape is also dependant on the EMA.[4]

---

* Official contribution of the National Institute of Standards and Technology; not subject to copyright in the United States of America.

§ To whom correspondence should be addressed: hae-jeong.lee@nist.gov

Metrology, Inspection, and Process Control for Microlithography XXII, edited by John A. Allgair, Christopher J. Raymond
Proc. of SPIE Vol. 6922, 692224, (2008) · 0277-786X/08/$18 · doi: 10.1117/12.772849

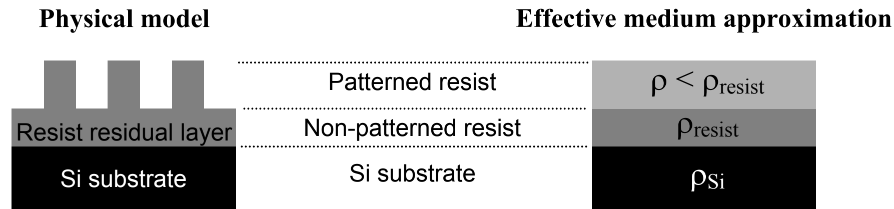

Figure 1. The cartoons illustrate both the physical structure of patterned resist and the effective medium approximation (EMA) model used to interpret the SXR data. The patterns are fabricated with imprint lithography.

Previous studies on periodic patterns showed that this SXR metrology is applicable for patterns with periodicities as large as 900 nm to 25 μm, depending on whether the incident X-rays are parallel or perpendicular, respectively, to the grating axis. Here we extend this study to the characterization of non-periodic or irregular patterns that would be more representative of the large patterned areas in a semiconductor device. In this case diblock copolymer films are used as a model system to create random two dimensional patterns without long range order. A diblock copolymer consists of two different linear polymers covalently connected at a single junction into a single chain molecule. When the two blocks are symmetric in their length but dissimilar chemical composition, the material will self assemble into a lamellar structure with alternating layers of the two blocks. One of the blocks usually has a stronger preference to wet the surface of a silicon wafer, resulting in the lamella being parallel to the surface in a thin film structure.[5,6] This preferred orientation causes a quantization of the film height to $(n + 1/2)\ L_o$, where L_o is the bulk value of the copolymer lamellar period and n is an integer. The layer at the top surface of the film only forms a smooth film if the volume of the material in the film is commensurate with a uniformly flat surface. If it is incommensurate the top layer becomes terraced with discrete islands, a bicontinuous structure, or holes with the integral height of L_o. In this manuscript we apply SXR to the symmetric diblock copolymer thin films with irregularly shaped terraces to determine if SXR is capable to characterize non-periodic patterns as a pattern shape metrology. We will discuss the structural characteristics on the terraces and the ordered lamellar layers as a function of the film thickness direction along with the scanning force microscope (AFM) results.

2. EXPERIMENTAL

Symmetric diblock copolymer films were prepared to investigate applicability of SXR to irregular patterns without periodicities. Poly(styrene-*b*-methyl methacrylate) (PS-*b*-PMMA, 25k to 26k) and poly(styrene-*b*-2vinylpyridine) (PS-*b*-PVP, 25.5k to 23.5k) were purchased from Polymer Source, Inc* and used as received. Block copolymers (BCPs) were dissolved in toluene at the concentration of 2 % by mass and the solutions were spin-coated at 262 rad/s (2500 rpm) to 314 rad/s (3000 rpm) onto smooth Si substrates. As-spun films were annealed at 180 °C for 24 h in the vacuum oven where they self-assemble into their layered lamellar structures. Thin film surface morphology and cross sectional profiles were characterized using a Dimension 3100 scanning force microscope (AFM, Digital Instruments, Inc.) in tapping mode.

The SXR measurements were performed on a Phillips X'pert diffractometer with a θ-2θ configuration at ambient temperature. A beam of Cu-Kα radiation with wavelength of 1.54 Å was directed with a focusing mirror through a four-bounce Ge (220) crystal monochromator onto the patterned films. The reflected beam was collected through a three bounce channel-cut Ge (220) crystal and directed into the solid-state detector mounted on a goniometer that has an angular reproducibility of ± 0.0001°.[7] All measurements were performed in the specular condition, where the grazing incidence angle (θ_i) of X-ray beam equals to the reflected angle into the detector (θ_r). The ratio of the reflected (I) to the incident (I_0) beam intensity defines the reflectivity ratio R. The reflectivity collected over a range of incident angles is plotted as a function of log (R) versus the scattering vector q, where $q = 4\pi/\lambda \sin(\theta_i)$ where λ is the X-ray wavelength. At low q the reflectivity is smooth until a sharp drop in the reflectivity occurs at the critical wave

* Certain commercial materials and equipment are identified in this paper in order to specify adequately the experimental procedure. In no case does such identification imply recommendation by the National Institute of Standards and Technology nor does it imply that the material or equipment identified is necessarily the best available for this purpose.

vecotor, q_c, where the X-rays first begin to penetrate into the film. The magnitude of q_c^2 is proportional to the total electron density ρ_e of the film through the expression: $q_c^2 = 16 \pi r_o \rho_e$ where r_o is the classical radius of an electron. The electron density profile perpendicularly through the plane of the film can be deduced by modeling the SXR data as mentioned earlier.[8] Here this modeling reveals the electron density of the patterned layers as a function of pattern height.

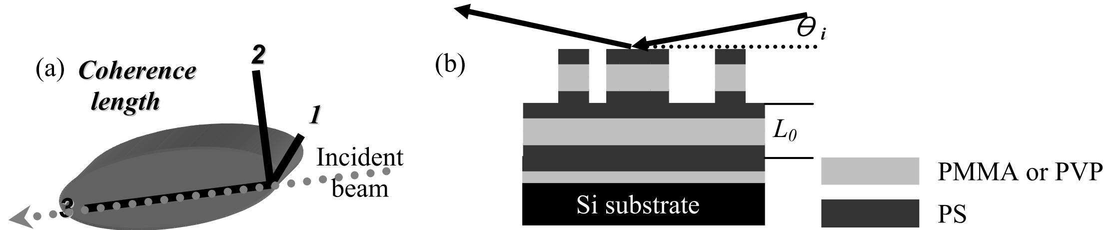

Figure 2. (a) In this cartoon the ellipsoidal feature schematically represents the effective coherence volume of the X-ray source in the different directions relative to the incident beam. Direction 3 coincides with the incident beam but 1 and 2 are orthogonal. Part (b) illustrates the hypothetical vertical structures of diblock copolymer model system after quantization resulting layer structures. Samples used in this study are not commensurate to complete the flat surface, inducing terrace of height L_0.

3. RESULTS AND DISCUSSION

From the previous study, we concluded that the coherence volume of the X-ray beam from the National Institute of Standards and Technology (NIST) reflectometer is as large as 25 µm in the incident beam direction.[3] Direction 3 in the cartoon of Figure 2(a) corresponds to the path of the X-ray beam toward the sample and the coherence length is expected to be the greatest in this direction. This is because the 4 bounce crystal monochromator increases the coherence of the X-ray beam primarily in direction 3. Therefore NIST reflectometer is capable to characterize the gratings with alternating line and space structures up to approximately 25 µm in pitch. Since most of the lateral length scales of the patterns in current devices are in the order of nanometer to several tenths of nanometer, SXR can be used to characterize pattern structures through the film thickness direction. However, patterns in current device are complicated irregular structures. Therefore it is important to have the characterization tool to determine the irregularly shaped structures as a pattern shape metrology. To investigate the applicability of X-ray reflectometer dibolock copolymers are selected as a model system.

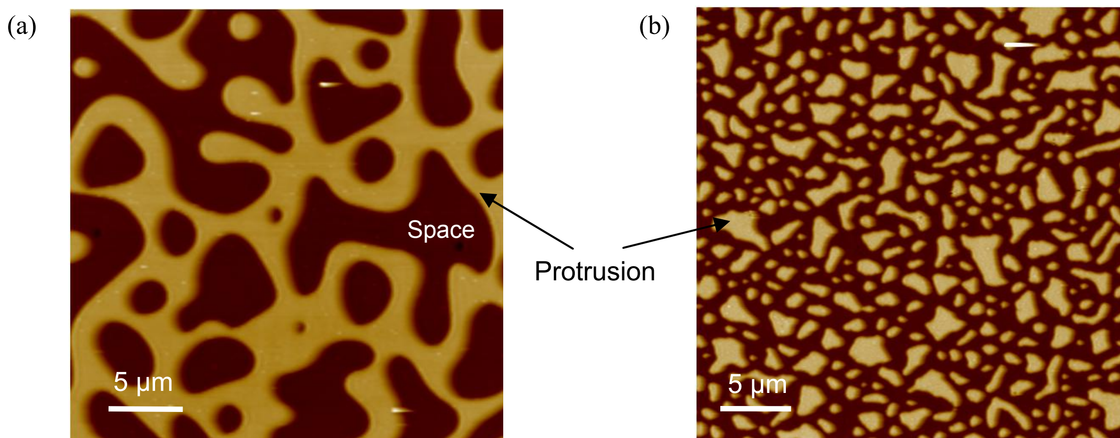

Figure 3. AFM images of (a) PS-*b*-PMMA (b) PS-*b*-PVP. Dark and bright regions are grooves recessed (or air space between irregularly shaped patterns) and protrusion projected from the quantized flat surface, respectively.

Figure 3 displays AFM images of model BCP used in this study for comparing surface morphologies generated in two diblock copolymers films; one is PS-*b*-PMMA and the other is PS-*b*-PVP. For these samples, the initial film thickness is not commensurate to complete quantized flat surface, resulting bicontinuous terrace with height L_o on the quantized flat surfaces as depicted in Figure 2(b). Dark regions are grooves recessed from the top surface and bright regions are protrusion protruded from the quantized flat layer. It is well-known that PS prefers the polymer-air interface (free surface) while PMMA and PVP has an energetic preference for the substrate. Therefore one can anticipate the surface exposed to the air both in the protruded region and recessed region are to be PS. The terrace shape (island, bicontinuous, and hole) is presupposed by initial film thickness before annealing since those shapes are induced by commensurability of polymeric material. PS-*b*-PVP has bicontinuous terraces with some islands, which indicates that thickness of initial film is slightly thicker than that needed for generating island structure. PS-*b*-PMMA shows well developed bicontinuous morphology suggesting that quantity of polymer exceed amount required for generating island morphology. The lateral width of protruded region and space is also influenced by initial film thickness. The average distance from center of groove to center of neighboring groove (or domain size of each block) is much larger in PS-*b*-PMMA BCP film. The AFM images of both samples reveal that the lateral length scale meaning the distance from the groove to neighboring groove is much smaller than 25 μm, which is X-ray coherence length. Therefore if EMA is applicable to the irregular shaped patterns as like in regularly repeated gratings, SXR is able to extract structural information of terraced layers and flat quantized layers underneath terrace.

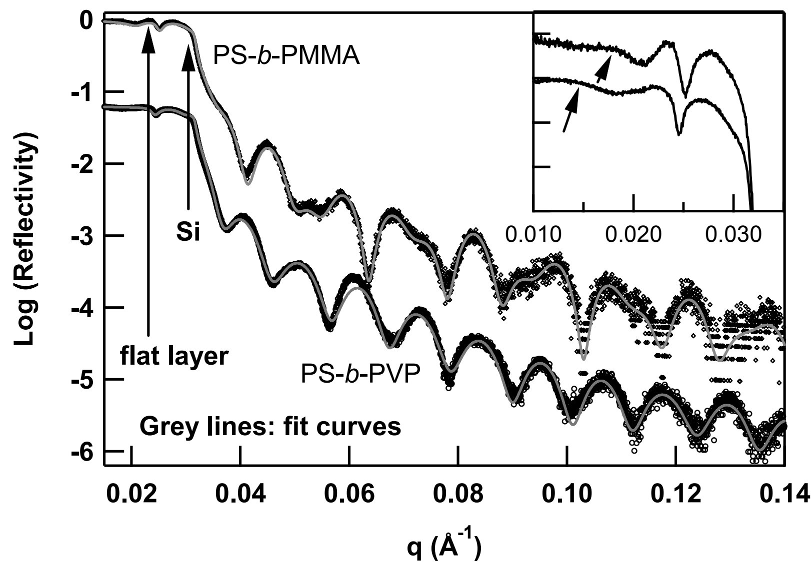

Figure 4. The X-ray reflectivity curves collected from diblock copolymers, PS-*b*-PMMA (◊) and PS-*b*-PVP (○) are plotted as a function of scattering wave vector, *q*. Grey lines are the best fit to the experimental data. Inset is the magnified data only for the lower *q* regime to compare the density of the terraced layers protruded on the surface of the flat quantized layer. Error bars are smaller than the size of symbols. Reflectivity curves are offset for clarity.

The experimental reflectivity data from two BCP thin films with bicontinuous structures are shown in Figure 4. Reflectivity curves resolve three critical angles, which show intensity drop in reflectivity. These results are evidence that the lateral variations in density between polymeric materials protruded and spaces separating them are averaged together, confirming that the EMA is applicable. The first critical wave vector corresponds to the lowest density layer of the EMA model, i.e., the terraced layer on the surface of the quantized flat layers. The inset of low *q* regime is added to examine clearly three critical wave vectors. The first critical wave vector of PS-*b*-PVP appears at lower *q* value and amplitude of critical wave vector is shallow compared to PS-*b*-PMMA. These results suggest that the terraced layer of PS-*b*-PVP has lower average density and thinner thickness than PS-*b*-PMMA. By recalling that the top layer of protruded terrace is PS in both BCP, the volume fraction of PS in the top layers of PS-*b*-PVP should be smaller than that of PS-*b*-PMMA. These results are consistent to the fact that PS-*b*-PVP has initially less materials (or

thin initial thickness) and induces early stage of bicontinuous morphology just starting to merge islands, while PS-*b*-PMMA generates well developed bicontinuous morphology. The quantitative volume fraction of each layer will be discussed in the later section. With further increases in q additional second and third critical wave vectors are encountered, which are corresponding to the density of flat layer and Si substrate, respectively. Each second and third critical wave vector appears at same q values regardless of BCP. Note that polymeric material exposed to air in flat layer is PS in both BCP and hence, the second critical wave vector in both BCP should be same. Complex reflectivity curves with multiple beating of interference fringes after the third critical wave vectors qualitatively imply multilayer structures through the film thickness direction.

We can quantitatively model the SXR data to obtain the detailed structural information of dimensions and shape as a function of film thickness. The smooth grey lines superimposed on the discrete symbols in Figure 4 are curves generated by the fit to the SXR data in terms of a multi-layer modeling algorithm. The density profiles corresponding to the best fits are plotted as a function of depth from the top surface exposed to the air toward silicon substrate as shown in Figure 5. The far left and right of the graph correspond to the free surface near the terraced layers and silicon substrate, respectively. The schematic cross-sectional polymeric layers are added to visualize quantized terrace and flat polymeric layers under the fit profiles. Rectangles in dark and bright grey color are PS and PMMA (or PVP), respectively. There are seven steps total in the SLD profiles, suggesting seven polymeric layers with different densities. Terraced and flat regions contain three and four layers with different SLD, respectively. These structures agree well with hypothetical BCP lamellar structures with alternating layers of the two blocks, which are symmetric in their length but dissimilar chemical composition.

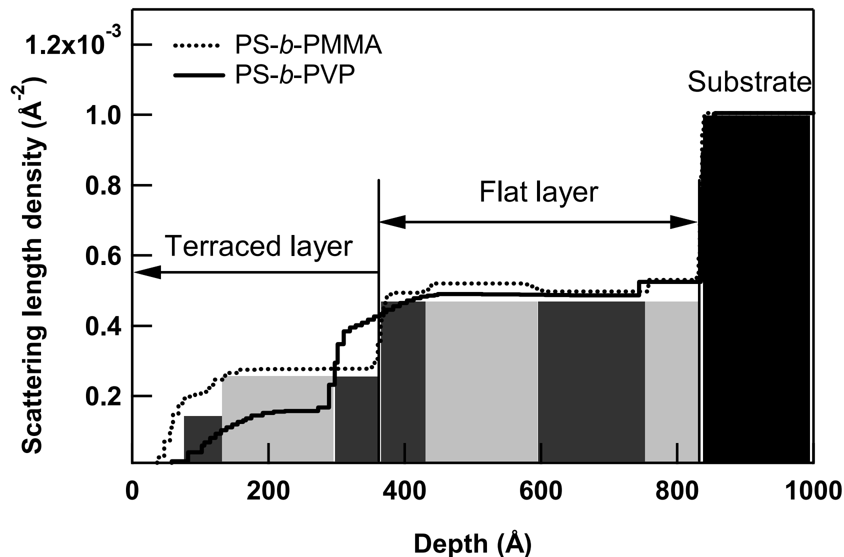

Figure 5. The scattering length density (SLD) profiles as a function of distance z through the films correspond to the fits to the reflectivity data presented in Figure 4.

Theoretically, brush layer of 0.5 L_0 thick, quantized flat layer of L_0 thick and terraced layer of L_0 thick are developed on Si substrate, sequentially. Total film thicknesses of PS-*b*-PMMA and PS-*b*-PVP turn out to be (780 ± 5) Å and (740 ± 5) Å, which are comparable to theoretical values for block copolymer with given molecular mass. Therefore, lamellar periods of BCP are 310 Å for PS-*b*-PMMA and 300 Å for PS-*b*-PVP, respectively. By comparing SLD in flat region, SLD of PS, $(0.492 \pm 0.05) \times 10^{-3}$ Å^{-2} is revealed to be slightly lower value than those of PMMA, $(0.525 \pm 0.05) \times 10^{-3}$ Å^{-2} and PVP, $(0.507 \pm 0.05) \times 10^{-3}$ Å^{-2}. As qualitatively anticipated from the differences in values between the first and second critical wave vectors in SXR curves, SLD in terraced layer dramatically decreases through the boundary between flat layer and terraced layer. However, the shapes of SLD profile in terraced layers show large difference for two BCP samples. For PS-*b*-PVP, the first two layers (near free surface) of terraced region shows much lower density, while the third layer of terraced region (next to flat layer) has much higher SLD compared to PS-*b*-PMMA. Large differences in density from top through bottom within terraced layer indicate large differences in lateral

fraction of polymeric materials to the space as a function of terrace height for PS-*b*-PVP sample. This result suggests patterns of trapezoidal shape with higher sidewall angle in cross-sectional view.

The volume fraction of polymeric material to the space in each layer of terraced structure is quantitatively calculated by comparing SLD of each layer in the terraced region to that in flat region through a rule of mixture: SLD_i (terraced layer) = SLD_i (flat layer) × (1 - $f_{space, i}$) + SLD (air) × $f_{space, i}$. Here, SLD (terraced layer), SLD (flat layer), and SLD (air) (equal to zero) correspond to the SLD of the terraced layer, flat layer, and air, respectively. f_{space} and i indicate volume fraction of space separating polymeric materials and polymer blocks such as PS, PMMA, and PVP. To calculate a volume fraction of each polymeric block in terraced layer, the SLD of the same block in the flat layer is used. As predicted from SLD profile, PS-*b*-PMMA has relatively smaller differences in volume fraction as a function of terrace height from (39 ± 2) % to (56 ± 2) %, while PS-*b*-PVP shows larger differences from (22 ± 2) % to (78 ± 2) %. Therefore, fractions of top layers to the base layers in trapezoid structure of terrace are approximately 70 % and 28 % for PS-*b*-PMMA and PS-*b*-PVP, respectively. Height of terrace for PS-*b*-PVP is (266 ± 5) Å, which is much shorter than estimated copolymer lamellar period. In contrast, PS-*b*-PMMA has terrace height similar to copolymer lamellar period, (309 ± 5) Å. These results are indicated in the amplitude of the first critical wave vectors in Figure 4.

To confirm cross-sectional profile determined from SXR data, 2 dimensional cross-sectional depth profiles are measured using the AFM images at several different spots. Figure 6 displays one of results analyzed for each BCP sample. The fraction of top layer to the base layer in terrace for PS-*b*-PMMA is approximately 71 %, which is higher than that for PS-*b*-PVP, approximately, 43 %. This result clearly shows that the terraced structure of PS-*b*-PMMA is more close to rectangle structure, while PS-*b*-PVP generates a trapezoid with steeper sidewall angle after annealing under same condition. Using AFM software, fractions of polymeric materials in terraced layer as a function of height through terraced layer are determined to compare to the fraction calculated from SXR fit. AFM images of 30 μm × 30 μm in Figure 3 are used to calculate average volume fraction, which is much smaller sample size used for SXR measurements, 1 cm × 1 cm. However, comparable results are obtained from both techniques. For PS-*b*-PMMA, volume fractions of polymers are (39 ± 5) %, (52 ± 5) %, and (55 ± 5) % from top to bottom in terraced layers respectively, which are in good agreement with SXR results, (39 ± 2) %, (53 ± 2) %, and (56 ± 2) %. Figure 7 is the result of volume faction of the second layer in terraced layer of PS-*b*-PMMA. Here, 'bearing area %' encompassed with thick rectangle indicates a volume fraction of polymer at the height pointed by the arrow in the right bottom figure.

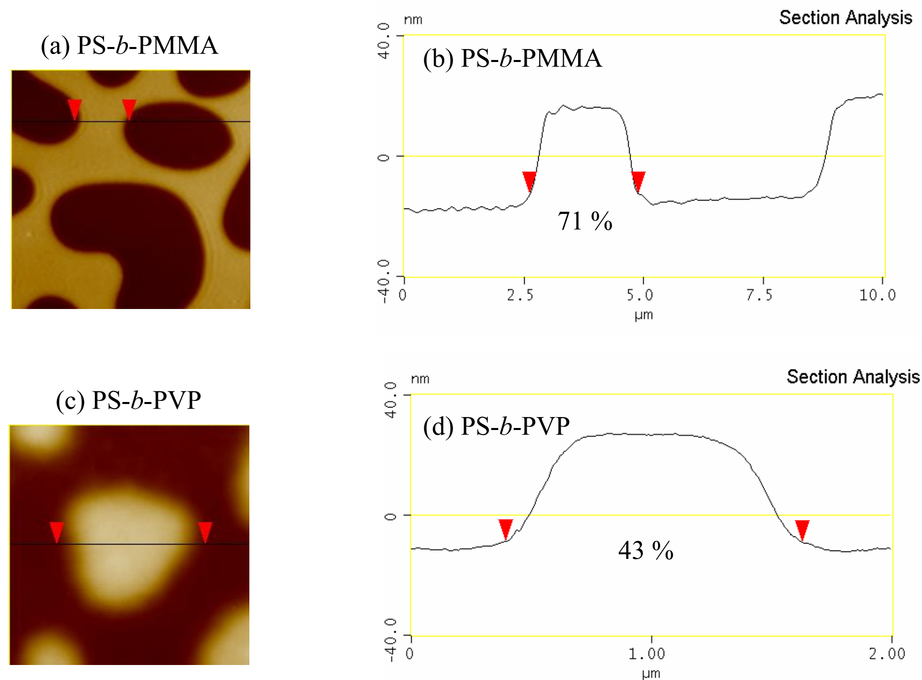

Figure 6. AFM images of (a) PS-*b*-PMMA and (c) PS-*b*-PVP. Part (b) and part (d) are 2D cross-sectional depth profiles obtained from AFM images in (a) and (c).

Box area	865.30 µm²
Center line av	45.069 nm
Bearing area	451.66 µm²
Bearing area %	**52.197**
Bearing depth	47.931 nm
Bearing volume	8.828 µm³
Hist area	12.705 µm²
Hist %	1.468
Hist depth	25.325 nm

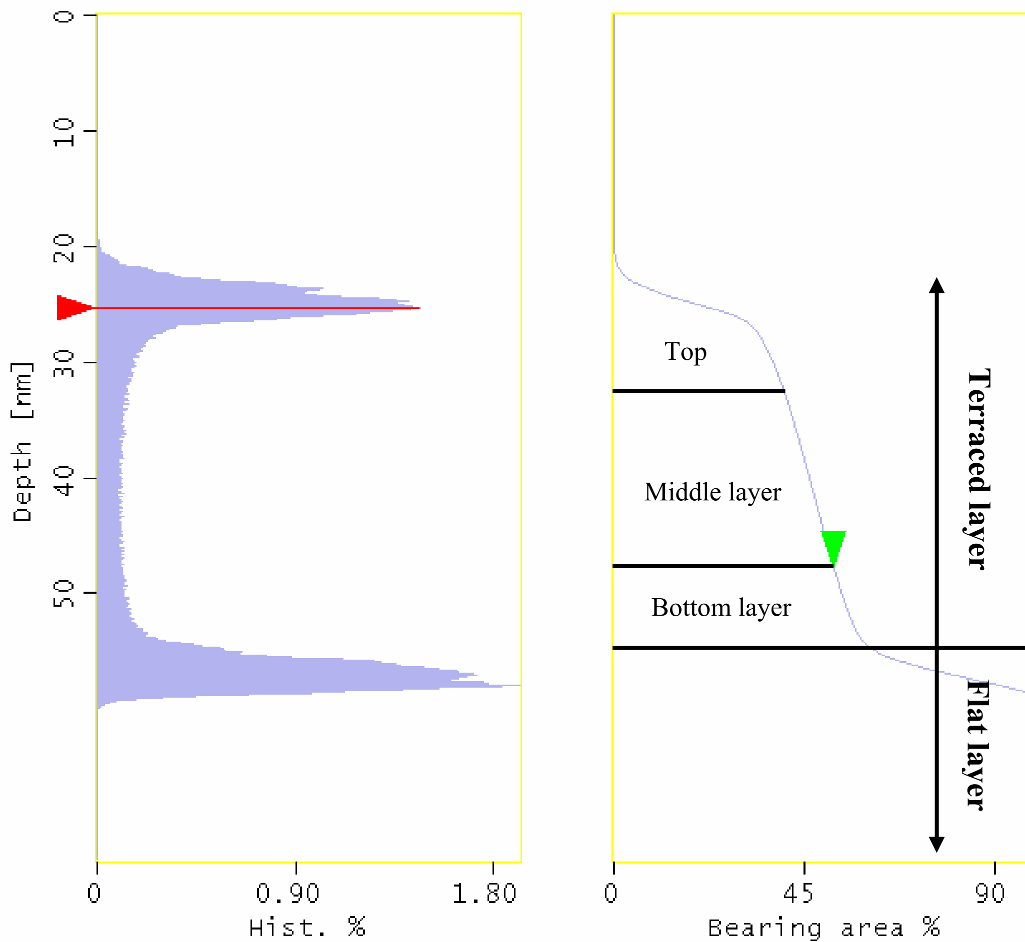

Figure 7. Calculation of volume fraction of polymeric material in terraced layer using AFM image in Figure 3(a), PS-*b*-PMMA. Bearing area % encompassed with thick rectangle indicates a volume fraction of polymer at the height pointed by the arrow in the right bottom figure.

4. CONCLUSION

Specular X-ray reflectivity (SXR) is reported as a powerful tool to quantify the shape or cross-section of periodic patterns. However, its use as a shape metrology depends upon the validity of the effective medium approximation (EMA). As long as the coherence length of the X-ray source is larger than the characteristic length scale of the patterns being characterized, the EMA appears to be valid. In the previous studies, we determined that the coherence length of the X-ray source in the incident beam direction is approximately 25 μm and hence SXR is capable to analyze periodic line gratings up to 25 μm. However, it is essential to have a metrology capable of analyzing irregularly shaped patterns since most of pattern structures encountered in current electronic devices are irregular and complicated random structures. Here we used diblock copolymers as a model system to generate irregularly shaped patterns, where two blocks are symmetric in their length but dissimilar chemical composition. Such a block copolymer self assembles into a lamellar structure with alternating layers of two blocks. Additionally, when initial film thickness is not commensurate to complete flat quantized lamellar structures, top layer becomes terraced structure such as island, bicontinuous and hole. We utilize quantized bicontinuous structures to confirm that the EMA is still applicable and SXR can be extended to irregularly shaped patterns. The lateral dimensions (i.e., distances between a groove and neighboring groove) are much smaller than X-ray coherence length of 25 μm. Detailed structural information is reported including volume fraction of terraced structures as a function of terrace height and cross-sectional profiles. By comparing the structural characteristics from SXR to AFM images of the in-plane surface morphology and cross-sectional profiles, we conclude that SXR can be a powerful tool for characterizing the shape profile of irregular as well as periodic patterns.

5. ACKNOWLEDGEMENT

The authors acknowledge the NIST Office of Microelectronics and the ATP Intramural Funding Program for their financial support.

6. REFERENCES

1. Lee, H. J., Soles, C. L., Ro, H. W., Kang, S., Jones, R. L., Lin, E. K., Karim, A., Wu, W. L. and Hines, D. R., "X-ray reflectivity and scattering for pattern shape metrology" Proc. SPIE Int. Soc. Opt. Eng. 6518, p. 651813-1 ~ 651813-8 (2007).
2. Lee, H. J., Soles, C. L., Ro, H. W., Jones, R. L., Lin, E. K., Wu, W. L., and Hines, D. R., "Nanoimprint pattern transfer quality from specular X-ray reflectivity", Appl. Phys. Lett. 87, 263111 (2005).
3. Lee, H.J., Soles, C. L., Kang, S., Ro, H. W., Lin, E. K. and Wu, W. L., "X-ray Reflectivity Measurements of Nanoscale Structures: Limits of the Effective Medium Approximation", American Institute of Physics (AIP) Conf. Proc., Frontiers of Characterization and Metrology for Nanoelectronics, 209-215 (2007).
4. Kim, T. J., Ghong, T. H., Kim, Y. D., Aspnes, D. E., Klein, M. V., Ko, D-S., Kim, Y-W., Elarde, V. C. and Coleman, J. J., "Investigation of effective-medium approximation, alloy, averagecomposition, and graded-composition models for interface analysis by spectroscopic ellipsometry", J. Appl. Phys. 102, 063512 (2007).
5. Bates, F. S. and Fredrickson, G. H., "Block Copolymer Thermodynamics: Theory and Experiment" Annu. Rev. Phys. Chem. 41, 5252 (1990).
6. Anastasiadis, S. H., Russell, T. P., Satija,S. K. and Majkrzak, C. F., "The morphology of symmetric diblock copolymers as revealed by neutron reflectivity", J.Chem. Phys. 92, 5677 (1990).
7. The data throughout the manuscript are presented along with standard uncertainty (±) involved in the measurement based on one standard deviation.
8. Parratt, L. G.,"Surface studies of solids by total reflection of X-rays", Phys. Rev. 95, 359 (1954).